crystals

MDPI

Article

Synthesis of Furan-Substituted *N*-Heteroacene-Based Liquid Material and Its Acid-Recognizing Behavior

Kyosuke Isoda [1,2,*] and Ayumi Ikenaga [3]

1 Program in Advanced Materials Science, Faculty of Engineering and Design, Kagawa University, 2217-20 Hayashi-cho, Takamatsu 761-0396, Japan
2 Health Research Institute, National Institute of Advanced Industrial Science and Technology (AIST), 2217-14 Hayashi-cho, Takamatsu 761-0395, Japan
3 Advanced Materials Science, Faculty of Engineering, Kagawa University, 2217-20 Hayashi-cho, Takamatsu 761-0396, Japan; s18g551@stu.kagawa-u.ac.jp
* Correspondence: k-isoda@eng.kagawa-u.ac.jp; Tel.: +81-87-864-2395

Received: 25 December 2018; Accepted: 15 January 2019; Published: 17 January 2019

Abstract: In this study, we synthesized a novel *N*-heteroacene-based liquid material 6,7-bis(3,7,11-trimethyl-1-dodecyloxy)-2,3-difurylquinoxaline (RP*N*L 1), containing two furan rings. We revealed that RP*N*L 1 adopted a disordered liquid at 25 °C, determined by polarized optical microscopic observation, differential scanning calorimetry, and X-ray diffraction measurements. The fluorescent spectrum measurement revealed that RP*N*L 1 showed a blue emission at 25 °C. Dissolving benzene sulfonic acid (BSA) in RP*N*L 1 brought about dramatic changes in its physical properties, such as emission colors, as well as sample states. Upon recognizing BSA, photoluminescent color was changed into orange, as well as phase transition occurred from liquid to a liquid-crystalline phase. RP*N*L 1 can function as an acid-recognizing material, accompanied with the color changes in emission.

Keywords: *N*-heteroacene; room-temperature π-conjugated liquid; acid-recognizing liquid; fluorescent liquid; fluorescent liquid crystal

1. Introduction

Stimuli-responsive soft functional materials get much attention because these materials can respond to external stimulus to show dramatic changes in physical properties, such as emission color and shape, in fact, these materials can adopt more than two independent conditions, which are expected to be applied into optoelectronic devices, such as sensors, energy devices, and actuators [1–5]. Recently, a lot of chemists have focused and developed a stimuli-responsive, solid-state luminescent materials response to various external stimuli, such as temperature, light, mechanical stress, and vapor, to give rise to dramatic changes in luminescent colors [6–10]. These solid materials are facile to fabricate film states by a coating technology, however, films fabricated from solid-state materials have a possibility to form unexpected defects, such as grain boundary and contact resistance on electrode, which should remarkably lead to a decrease in their efficiency. If stimuli-responsive liquid materials are developed instead of solid-state materials, the disadvantages mentioned above are expected to be resolved, and the research field of stimuli-responsive materials will further expand. Herein, we report on a novel, room-temperature-photoluminescent, π-conjugated liquid (RPL) material, involving a stimuli-responsive behavior, itself.

Recently, RPL materials have been reported by some groups, which have been classified into novel, functional soft materials [11–18]. Nakanishi's group has reported many liquid materials composed of polyaromatic hydrocarbons (PAH), such as naphthalene, anthracene, pyrene, and phenylenevinylene.

Additionally, our group has reported a room-temperature-photoluminescent *N*-heteroacene-based liquid (6,7-bis(3,7,11-trimethyl-1-dodecyloxy)-2,3-difurylquinoxaline or (RP*N*L)) [13,18]. *N*-heteroacene partially contains sp^2 imino-*N* atoms instead of sp^2 carbon atoms, [19–25] which can recognize a Lewis acid, such as a proton or metal ion, because imino-*N* atoms with lone-pair electrons serve as a Lewis base. The recognition of proton for imino-*N* atoms can give rise to an obvious change in the electronic property of the *N*-heteroacene framework [13,18,25]. Accordingly, RP*N*L itself can function as an acid-recognizing material, in contrast to RPL composed of a PAH framework. In this study, we prepare novel RP*N*L 1, containing two furan rings. Although our group has reported thiophene-appended PR*N*L materials [18], it is important to investigate an influence on the electronic properties, as well as the acid-recognizing behavior, by substitution of various aromatic rings, leading to a sophisticated molecular design and tailor-made synthesis, for the development of novel PR*N*L materials with fine-tuned characters. Moreover, we investigated the theoretical calculations on electronic property, as well as a structure for furan-appended PR*N*L material, by using density functional theory (DFT) calculations.

2. Materials and Methods

2.1. General Methods

^{1}H and ^{13}C NMR spectra were recorded on a Varian UNITY INOVA400NB spectrometer (Varian, Palo Alto, CA, USA). Chemical shift of ^{1}H and ^{13}C NMR signals were quoted to tetramethylsilane (δ = 0.00) and (δ = 77.00) as internal standards, respectively. FT-IR spectra were measured with a Perkin-Elmer Spectrum Two FT-IR Spectrometer (Perkin Elmer, Waltham, MA, USA). (Fast Atom Bombardment-Mas Spectrometry) FAB-MS mass spectra were collected on a JEOL JMS-AX505H (JEOL, Tokyo, Japan). UV–vis absorption spectra were recorded with a Perkin-Elmer Lambda35 UV–vis Spectrometer (Perkin Elmer, Waltham, MA, USA). Fluorescent (FL) spectra were recorded with a Perkin-Elmer LS45 Luminescence Spectrophotometer (Perkin Elmer, Waltham, MA, USA). XRD patterns were obtained with a SHIMADZU XRD-6100 X-RAY DIFFRACTOMETER (SHIMADZU, Kyoto, Japan), using Ni-filtered Cukα radiation. The density functional theory (DFT) calculations were carried out using Wavefunction SPARTAN'18 programs (Wavefunction, Inc., Irvine, CA, USA). The ground-state geometries were optimized at the B3LYP/6-31G* level of theory [26–28]. All reagents and solvents were purchased from Wako, Tokyo Kasei, Kanto Chemical, or Aldrich, and used as received. 4,5-bis(3,7,11-trimethyl-1-dodecyloxy)-1,2-dinitrobenzene was prepared, according to the procedures of the literature [18]. 6,7-bis(3,7,11-trimethyl-1-dodecyloxy)-2,3-difurylquinoxaline·benzene sulfonic acid (RP*N*L 1·BSA) was prepared by dissolving RP*N*L 1 and BSA in $CHCl_3$, followed by evaporation of $CHCl_3$ under vacuum. The $CHCl_3$ solution of RP*N*L 1 with HCl was prepared by an addition of a drop of HCl (35.0–37.0%), into the $CHCl_3$ solution of RP*N*L 1.

2.2. Synthesis of 6,7-bis(3,7,11-trimethyl-1-dodecyloxy)-2,3-difurylquinoxaline (RPNL 1)

To a suspension of 4,5-bis(3,7,11-trimethyl-1-dodecyloxy)-1,2-dinitrobenzene (0.62 g, 1.0 mmol) and Pd/C (0.15 g), in dry EtOH (80 mL), at 0 °C, hydrazine monohydrate was added dropwise (40 mL). After reflux for 2 h, the reaction mixture was filtrated through Celite, under Ar, and then evaporated. The crude product was heated with 1,2-di(2-furyl)ethane-1,2-dione (0.23 g, 1.2 mmol) in dry EtOH (40 mL), under Ar, for 24 h. The reaction mixture was cooled to 25 °C and extracted with $CHCl_3$, three times. The combined organic layers were washed with water, and dried over anhydrous Na_2SO_4. After filtration and evaporation, the crude product was purified by column chromatography (silica, hexane/$CHCl_3$ = 4/1 (v/v)), and dried, under vacuum, to afford RP*N*L 1 as a yellow viscous liquid (0.44 g, 62%). UV/Vis ($CHCl_3$): λ_{max} (log ε) = 278(4.57), 396(4.38); IR(ATR): v = 2925, 2870, 1617, 1494, 1467, 1385, 1331, 1231, 1211, 1172, 1067, 1011, 995, 925, 898, 846, 813, 736, 594, and 492 cm^{-1}; ^{1}H NMR (400 MHz, $CDCl_3$): δ 7.60(m, 2H), 7.40(m, 2H), 6.54(m, 4H), 4.20(m, 4H), and 1.98–0.84(m, 66H) ppm; ^{13}C NMR (75 MHz, $CDCl_3$): δ 153.31, 151.19, 143.56, 140.12, 137.98, 111.68, 111.66, 107.11, 67.77, 39.35,

37.37, 27.28, 35.69, 35.63, 32.79, 30.13, 29.68, 27.95, 24.80, 24.38 22.69, 22.60, and 19.71 ppm; FAB-MS: m/z calcd: 715.06 $[M]^+$; found: 715.74.

3. Results and Discussion

For a molecular design of RP*N*L 1 to combine the inherently acid-recognizing property, it is indispensable that the two imino-*N* atoms are accessible from external stimuli, by other substituted moieties in RPNL 1, without any disturbance. Before synthesis of the RP*N*L 1, we performed DFT calculations to investigate the molecular structure of RP*N*L 1, by using the Spartan'18 software package (Wavefunction, Inc., Irvine, CA, USA). The optimized molecular geometry of the RP*N*L 1, calculated at the B3LYP/6-31G* level of theory, revealed that two long alkoxy chains did not interact with the imino-*N* atoms as acid-recognizing moieties in Figure 1a. Additionally, the interatomic distances between the O atoms on the furan rings and the imino-*N* atoms were 2.696 and 2.697 Å, which is shorter than the sum of van der Waals radius (O–N 3.07 Å), respectively [29]. This result suggests that interatomic interactions occur between the O atoms on the furan rings and the imino-*N* atoms pyrazine framework, as a result, the acid-recognizing capability of the imino-*N* atoms might decrease. Therefore, we also investigated the acid-recognizing capability of RP*N*L 1 to benzene sulfonic acid (BSA), with lower *p*Ka. DFT calculation of RP*N*L 1 with BSA revealed that the BSA molecule was capable of approaching one imino-*N* atom of RP*N*L 1, because the interatomic distance between the O atom of the BSA and the imino-*N* atom was accumulated to be 2.687 Å, in Figure 1b, despite a steric repulsion by the alkyl chains, as well as the furan rings. As a result of the hydrogen bonding, the distance between the O atom and the N atom were much shorter than the corresponding sum of the van der Waals radius. Moreover, the interatomic distance between the imino-*N* atom and the O atom for the furan ring, is almost the same as that before the recognition of the BSA. As a result, the non-bonding interaction between the imino-*N* atom and the O atom may be weak, which is expected, as the RP*N*L 1 can recognize an acid substance such as BSA.

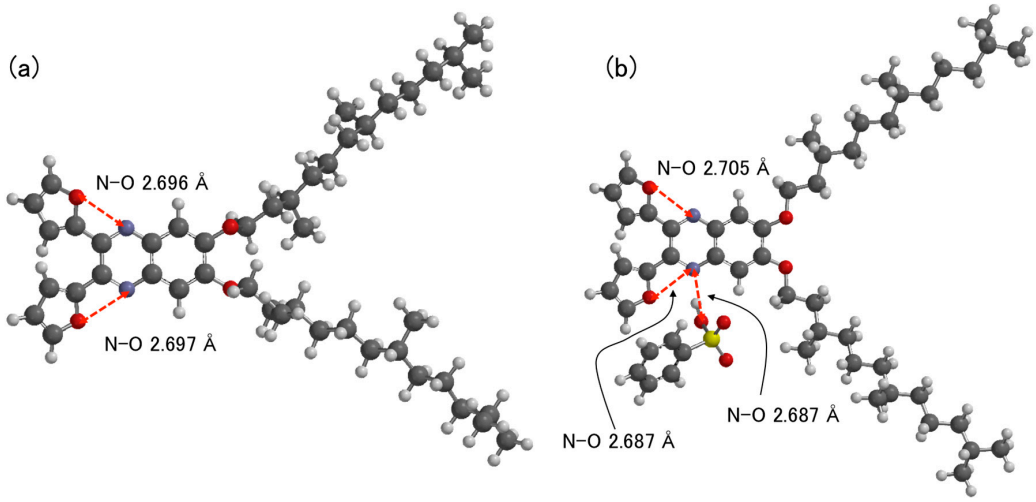

Figure 1. Top and side views of the optimized molecular geometry of (**a**) 6,7-bis(3,7,11-trimethyl-1-dodecyloxy)-2,3-difurylquinoxaline (RP*N*L 1) and (**b**) RP*N*L 1 with benzene sulfonic acid (BSA), as calculated at the B3LYP/6-31G* level.

We prepared a novel RP*N*L 1, containing two furan rings, in Scheme 1. 4,5-Bis(3,7,11-trimethyl-1-dodecyloxy)-1,2-dinitrobenzene was reduced with hydrazine monohydrate, using by Pd/C in dry EtOH, to obtain a diaminobenezene derivative unstable to air, then followed by thermal condensation with 1,2-di(2-furyl)ethane-1,2-dione, in dry EtOH, to afford RP*N*L 1. To study a fluidic liquid property of RP*N*L 1, polarized optical microscopic (POM) observation, differential scanning calorimetry (DSC), and X-ray diffraction (XRD) measurements were operated, as shown in Figures 2 and 3. POM observation of the

RP*N*L 1 at 25 °C, clarified that no birefringence was observed in Figure 2. Additionally, the XRD pattern of RP*N*L 1 at 25 °C showed no peak, due to the self-assembled structures and a halo peak organized from the molten-branched alkoxy chains in Figure 3. Both results strongly indicate that RP*N*L 1 is a fluidic liquid at 25 °C. DSC trace of RP*N*L 1 showed that no phase transition peak appeared from an isotropic liquid to a crystal, on first cooling and then heating. Additionally, glass transition temperatures (T_g) were observed to be at −35.5 °C on first cooling, and at −32.8 °C on heating, indicating that RP*N*L 1 adopted a liquid state in a wide temperature range, including up to 25 °C.

We added BSA (equimolar to RP*N*L 1) into RP*N*L 1 to investigate the dissolving behavior of RP*N*L 1. Upon heating at 100 °C, the BSA was dissolved in RP*N*L 1, whereas the POM observation of the RP*N*L 1·BSA (in which RP*N*L 1 dissolves BSA), showed birefringence, under a cross-Nicols condition, at 25 °C, in Figure 3; of which observation, the result was clearly different from that for RP*N*L 1. This result implies that RP*N*L 1 can recognize BSA to form a complex, via hydrogen bonding [18]. Moreover, an appearance of birefringence indicates that RP*N*L 1·BSA self-assemblies into the formation of an ordered structure. To confirm that a phase transition of RP*N*L 1 occurs by the addition of the BSA, we carried out the DSC measurements for the RP*N*L 1·BSA.

DSC measurements revealed that the T_g at 7.8 °C for RP*N*L 1·BSA was much higher than that at −32.8 °C for RP*N*L 1, and the melting point (T_m) clearly appeared at 44.3 °C on heating, as shown in Figure 3b. In particular, the appearance of the T_m strongly suggested that the phase transition of RP*N*L 1 would happen from a disordered liquid-to-liquid-crystalline (LC) state, by a complexation between RP*N*L 1 and BSA. The phase transition of RP*N*L 1 from a liquid state to an LC phase, by recognition of the BSA, was derived from the induction of polarity. Before recognition, RP*N*L 1 comprises aromatic moiety and aliphatic alkyl chains, which is a nonpolar molecule. On the other hand, the complexation of the RP*N*L 1 with the BSA generates a polarity because the RP*N*L 1·BSA becomes an amphiphilic molecule composed of ionic *N*-heteroacene framework, as well as hydrophobic alkyl chains. This dramatic change in a polarity of the aromatic moiety works as a driving force to self-assemble into an LC phase.

It is noted that the LC structure of the RP*N*L 1·BSA could be aligned by a mechanical shearing in the sandwiched glass substrates, in Figure 2, suggesting that the RP*N*L 1·BSA self-assembled to form the columnar LC phase. The direction of the long axis of the columns for the RP*N*L 1·BSA corresponds to the shearing direction, of which birefringence is alternately bright and dark, upon rotation by 45°, under the cross-Nicols condition. It is known that these phenomena are consistent with the RP*N*L 1·BSA forming the columnar LC phases, reported by other groups [30]. To investigate the self-assembled structure of the RP*N*L 1·BSA, the XRD pattern of the RP*N*L 1·BSA at 25 °C, was operated. The XRD pattern of the RP*N*L 1·BSA, showed three peaks at 42.1 (11), 38.4 (20), and 21.1 (31), in the small-angle region at 25 °C, as shown in Figure 3d, indicating that the RP*N*L 1·BSA self-assembled into the rectangular columnar (Col_r) LC structure, with the space group $C2/m$ [31]. We anticipated that each adjacent π-conjugated framework in the mixture of RP*N*L 1·BSA would adopt alternating inversion arrangements because of the acid recognition made by RP*N*L 1—an amphiphilic molecule—to induce the electrostatic interactions [18]. Moreover, an amphiphilic property of the RP*N*L 1·BSA induced nanosegregation to stabilize the Col_r LC phase.

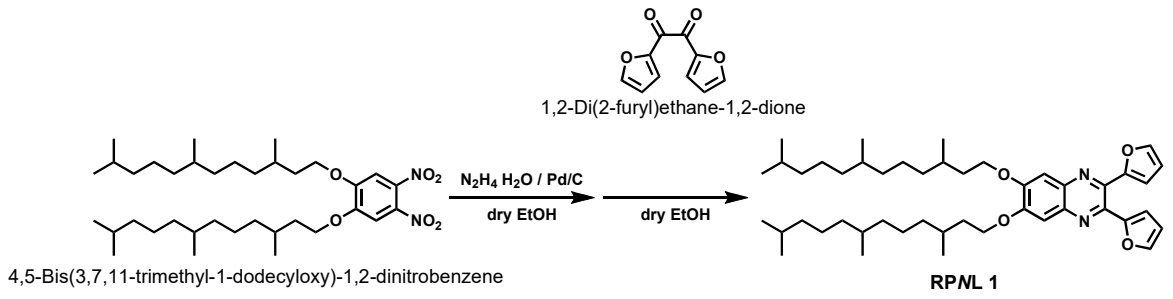

Scheme 1. Synthesis of RP*N*L 1.

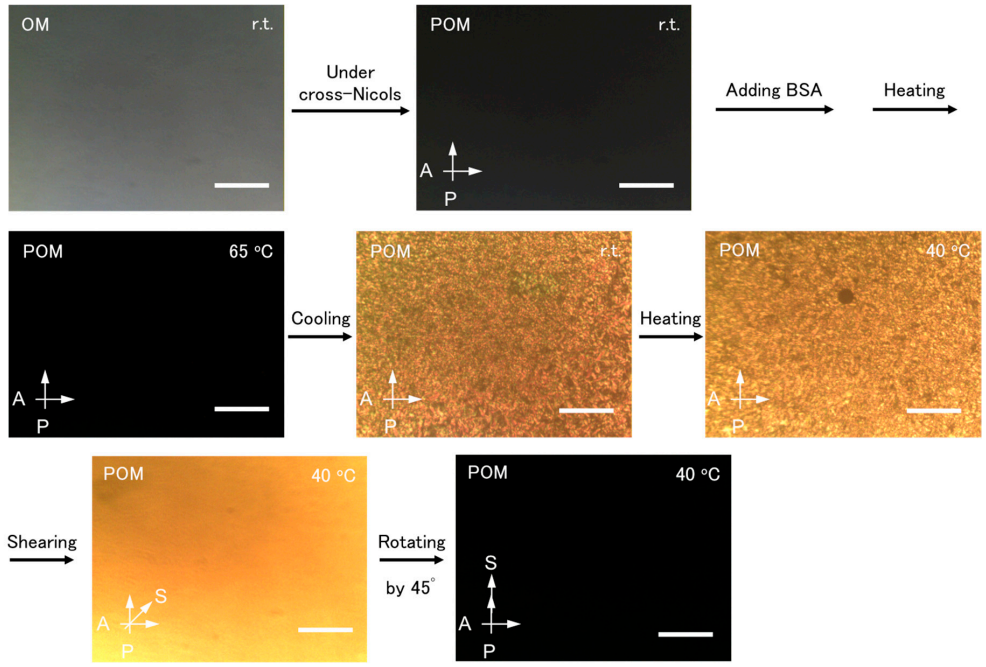

Figure 2. Photomicrographs of the optical microscopic (OM) and the polarized optical microscopic (POM) observations, the RP*N*L 1, and the RP*N*L 1·BSA. A, P, and S indicate the analyzer, polarizer, and shearing direction, respectively.

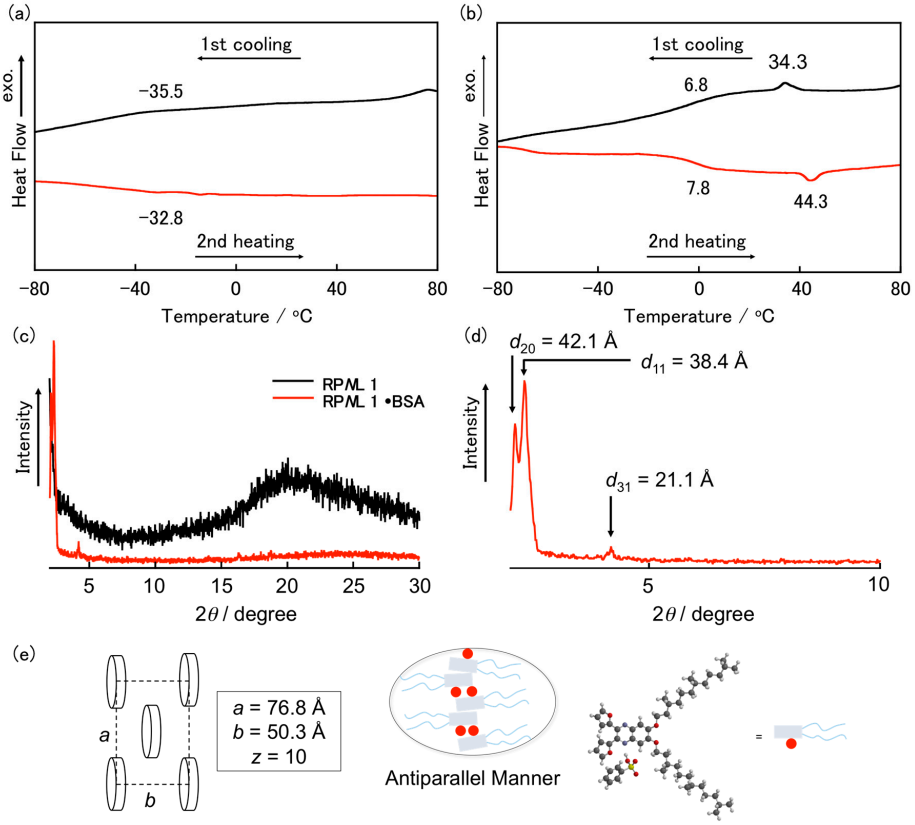

Figure 3. Differential Scanning Calorimetry (DSC) traces of the (**a**) RP*N*L 1 and (**b**) RP*N*L 1·BSA, on a scanning rate of 10 K/min; (**c**) XRD patterns of RP*N*L 1 and RP*N*L 1·BSA at 25 °C; (**d**) XRD pattern of the magnified view for RP*N*L 1·BSA; and (**e**) Predicted schematic illustration of the molecular packing for RP*N*L 1·BSA in a disc-like stratum of a column.

Then, to evaluate the electronic properties of the RP*N*L 1 and RP*N*L 1·BSA, we carried out UV-vis absorption and FL spectra measurements, due to the ground and excited states, respectively. In a liquid state, the UV-vis absorption spectrum of RP*N*L 1 showed two peaks at 277 and 392 nm, in Figure 4a, which was almost same as that of RP*N*L 1, in a $CHCl_3$ solution in Figure 4c. The FL spectrum of RP*N*L 1 showed a broad peak at 456 nm in a liquid state, in which the photoluminescent color was blue, Figure 4b. Compared to the peak, around at 450 nm, in the FL spectrum of RP*N*L 1 in a $CHCl_3$ solution (10^{-3}–10^{-6} M), that of RP*N*L 1 in a liquid state was bathochromically shifted. These results suggest that molecules at an excited state in a condensed liquid should bring about a weak electronic coupling, via an intermolecular interaction with each other. Additionally, an electronic coupling between the molecules at ground state, was weak.

Dissolving BSA in RP*N*L 1 gave rise to remarkable changes in the UV-vis absorption and the FL spectra. In a condensed state, the UV-vis absorption spectrum of the RP*N*L 1·BSA showed two peaks at 297 and 465 nm. In particular, the peak of longer wavelength for RP*N*L 1·BSA was red-shifted by protonation, compared to that of RP*N*L 1. Additionally, the color of RP*N*L 1 clearly changed from light yellow to orange. The UV-vis absorption spectrum of RP*N*L 1 with HCl in the $CHCl_3$ solution (10^{-3}–10^{-6} M) was 468 nm, which was almost the as same that of RP*N*L 1·BSA in a condensed state, in which the behavior was consistent with that before complexation between RP*N*L 1 and BSA.

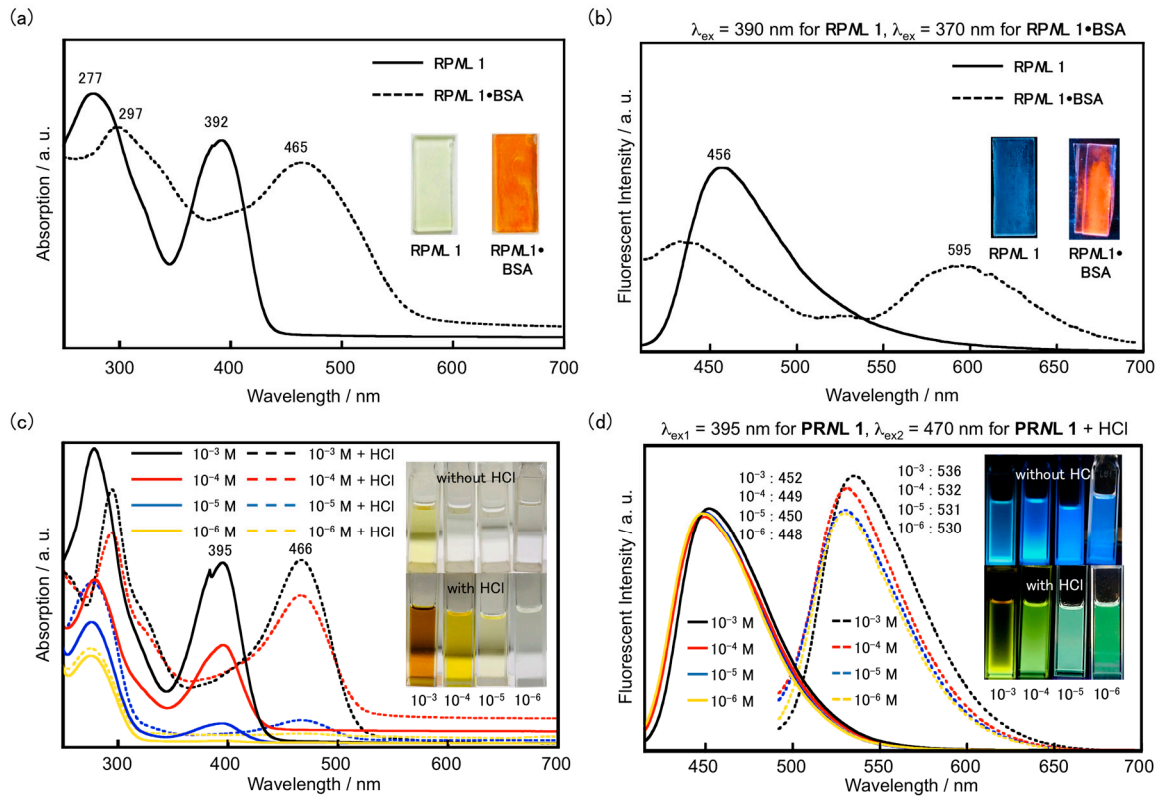

Figure 4. (**a**) UV-vis absorption spectra and (**b**) fluorescent spectra of RP*N*L 1 and RP*N*L 1·BSA. (**c**) UV-vis absorption spectra and (**d**) fluorescent spectra of RP*N*L 1 and RP*N*L 1 with HCl in $CHCl_3$ solutions. Photographs of (**a**) and (**c**) under room light and (**b**) and (**d**) under black light (365 nm).

It should be noted that the peak FL spectrum for RP*N*L 1·BSA was much red-shifted by ca. 140 nm. The blue emission for RP*N*L 1 clearly turned into an orange emission by protonation. On the other hand, the FL spectrum of RP*N*L 1 with HCl in the $CHCl_3$ solution (10^{-3}–10^{-6} M) showed a peak at around 530 nm, with a light green emission, which clearly differed from that of RP*N*L 1·BSA in the condensed state. The remarkable red-shift for the RP*N*L 1·BSA, in a condensed state, contributed to the strong electronic coupling between molecules, because the induction of polarity should enhance the

intermolecular interaction, leading to a tightly molecular packing for RP*N*L 1·BSA, in the condensed Col_r LC state. These pronounced changes by acid recognition were derived from RP*N*L 1, as a liquid material, in a condensed state, and not observed as a solution state. The dramatic changes in the fluorescent colors were advantages characteristic of a condensed liquid material.

4. Conclusions

We prepared novel RP*N*L 1 comprising of two furan rings. Dissolving BSA in RP*N*L 1 gave rise to the remarkable change in physical properties of RP*N*L 1, such as electronic properties, as well as sample condition. Upon complexation with BSA, the photoluminescent color of blue emission for RP*N*L 1 turned into an orange emission. Additionally, the phase transition happened from a disordered liquid state to a self-organizing columnar LC phase. As a result, RP*N*L 1 can function as an acid-responsive material. Further investigations of the various PR*N*Ls showing functionality and stimuli-responsive capability are in progress, in our laboratory.

Author Contributions: A.I. synthesized RP*N*L 1 and carried out all experiments. K.I. designed and supervised this project, and wrote the manuscript.

Acknowledgments: This study was supported by the Japan Society for the Promotion of Science (JSPS) KAKENHI Grant Number 16H04095 and 18K05263, the Oil & Fat Industry Kaikan, the Izumi Science and Technology Foundation, and the Tokyo Kasei Chemical Promotion Foundation. We thank T. Kusunose at Kagawa University and A. Sonoda at the Health Research Institute, AIST for help with performing the DSC and NMR measurements.

Conflicts of Interest: The authors declare no conflict of interest.

References and Note

1. Chen, L.-J.; Yang, H.-B. Construction of Stimuli-Responsive Functional Materials Via Hierarchical Self-Assembly Involving Coordination Interactions. *Acc. Chem. Res.* **2018**, *51*, 2699–2710. [CrossRef] [PubMed]
2. Isapour, G.; Lattuada, M. Bioinspired Stimuli-Responsive Color-Changing Systems. *Adv. Mater.* **2018**, *30*, 1707069. [CrossRef] [PubMed]
3. Montero de Espinosa, L.; Meesorn, W.; Moatsou, D.; Weder, C. Bioinspired Polymer Systems with Stimuli-Responsive Mechanical Properties. *Chem. Rev.* **2017**, *117*, 12851–12892. [CrossRef] [PubMed]
4. Wang, H.; Ji, X.; Li, Z.; Huang, F. Fluorescent Supramolecular Polymeric Materials. *Adv. Mater.* **2017**, *29*, 1606117. [CrossRef] [PubMed]
5. Yan, X.; Wang, F.; Zheng, B.; Huang, F. Stimuli-Responsive Supramolecular Polymeric Materials. *Chem. Soc. Rev.* **2012**, *41*, 6042–6065. [CrossRef]
6. Löwe, C.; Weder, C. Oligo(P-Phenylene Vinylene) Excimers as Molecular Probes: Deformation-Induced Color Changes in Photoluminescent Polymer Blends. *Adv. Mater.* **2002**, *14*, 1625–1629. [CrossRef]
7. Mutai, T.; Satou, H.; Araki, K. Reproducible on-Off Switching of Solid-State Luminescence by Controlling Molecular Packing through Heat-Mode Interconversion. *Nat. Mater.* **2005**, *4*, 685–687. [CrossRef]
8. Qi, Z.; Schalley, C.A. Exploring Macrocycles in Functional Supramolecular Gels: From Stimuli Responsiveness to Systems Chemistry. *Acc. Chem. Res.* **2014**, *47*, 2222–2233. [CrossRef]
9. Sagara, Y.; Kato, T. Mechanically Induced Luminescence Changes in Molecular Assemblies. *Nat. Chem.* **2009**, *1*, 605–610. [CrossRef]
10. Sagara, Y.; Mutai, T.; Yoshikawa, I.; Araki, K. Material Design for Piezochromic Luminescence: Hydrogen-Bond-Directed Assemblies of a Pyrene Derivative. *J. Am. Chem. Soc.* **2007**, *129*, 1520–1521. [CrossRef]
11. Santhosh, B.S.; Aimi, J.; Ozawa, H.; Shirahata, N.; Saeki, A.; Seki, S.; Ajayaghosh, A.; Mohwald, H.; Nakanishi, T. Solvent-Free Luminescent Organic Liquids. *Angew. Chem. Int. Ed.* **2012**, *51*, 3391–3395. [CrossRef] [PubMed]
12. Santhosh, B.S.; Hollamby, M.J.; Aimi, J.; Ozawa, H.; Saeki, A.; Seki, S.; Kobayashi, K.; Hagiwara, K.; Yoshizawa, M.; Mohwald, H.; et al. Nonvolatile Liquid Anthracenes for Facile Full-Colour Luminescence Tuning at Single Blue-Light Excitation. *Nat. Commun.* **2013**, *4*, 1969.

13. Isoda, K.; Sato, Y.; Matsukuma, D. Fluorescent *N*-Heteroacene-Based π-Conjugated Liquid Responsive to Hcl Vapor. *Chem. Select.* **2017**, *2*, 7222–7226. [CrossRef]
14. Lu, F.; Takaya, T.; Iwata, K.; Kawamura, I.; Saeki, A.; Ishii, M.; Nagura, K.; Nakanishi, T. A Guide to Design Functional Molecular Liquids with Tailorable Properties Using Pyrene-Fluorescence as a Probe. *Sci. Rep.* **2017**, *7*, 3416. [CrossRef] [PubMed]
15. Lu, F.; Jang, K.; Osica, I.; Hagiwara, K.; Yoshizawa, M.; Ishii, M.; Chino, Y.; Ohta, K.; Ludwichowska, K.; Kurzydłowski, K.J.; et al. Supercooling of Functional Alkyl-ΠI Molecular Liquids. *Chem. Sci.* **2018**, *9*, 6774–6778. [CrossRef]
16. Lu, F.; Kitamura, N.; Takaya, T.; Iwata, K.; Nakanishi, T.; Kurashige, Y. Experimental and Theoretical Investigation of Fluorescence Solvatochromism of Dialkoxyphenyl-Pyrene Molecules. *Phys. Chem. Chem. Phys.* **2018**, *20*, 3258–3264. [CrossRef]
17. Narayan, B.; Nagura, K.; Takaya, T.; Iwata, K.; Shinohara, A.; Shinmori, H.; Wang, H.; Li, Q.; Sun, X.; Li, H.; et al. The Effect of Regioisomerism on the Photophysical Properties of Alkylated-Naphthalene Liquids. *Phys. Chem. Chem. Phys.* **2018**, *20*, 2970–2975. [CrossRef]
18. Sato, Y.; Mutoh, Y.; Matsukuma, D.; Nakagawa, M.; Kawai, T.; Isoda, K. Tuning the Electronic Properties and Acid-Response Behavior of *N*-Heteroacene-Based π-Conjugated Liquids by Changing the Number of ΠI-Conjugated Substituents. *Chem. Asian J.* **2018**, *13*, 2619–2625. [CrossRef]
19. Isoda, K.; Nakamura, M.; Tatenuma, T.; Ogata, H.; Sugaya, T.; Tadokoro, M. Synthesis and Characterization of Electron-Accepting Nonsubstituted Tetraazaacene Derivatives. *Chem. Lett.* **2012**, *41*, 937–939. [CrossRef]
20. Bunz, U.H.F.; Engelhart, J.U.; Lindner, B.D.; Schaffroth, M. Large *N*-Heteroacenes: New Tricks for Very Old Dogs? *Angew. Chem. Int. Ed.* **2013**, *52*, 3810–3821. [CrossRef]
21. Isoda, K.; Abe, T.; Tadokoro, M. Room-Temperature Redox-Active Liquid Crystals Composed of Tetraazanaphthacene Derivatives. *Chem. Asian J.* **2013**, *8*, 2951–2954. [CrossRef] [PubMed]
22. Isoda, K.; Abe, T.; Funahashi, M.; Tadokoro, M. Electron Transport of Photoconductive n-Type Liquid Crystals Based on a Redox-Active Tetraazanaphthacene Framework. *Chem. Eur. J.* **2014**, *20*, 7232–7235. [CrossRef] [PubMed]
23. Bunz, U.H.F. The Larger Linear *N*-Heteroacenes. *Acc. Chem. Res.* **2015**, *48*, 1676–1686. [CrossRef] [PubMed]
24. Isoda, K.; Abe, T.; Kawamoto, I.; Tadokoro, M. Self-Organized Superstructure and Electronic Properties of a Liquid-Crystalline Tetraazapentacene Derivative. *Chem. Lett.* **2015**, *44*, 126–128. [CrossRef]
25. Isoda, K. Acid-Responsive *N*-Heteroacene-Based Material Showing Multi-Emission Colors. *ChemistryOpen* **2017**, *6*, 242–246. [CrossRef] [PubMed]
26. Hariharan, P.C.; Pople, J.A. The Effect of D-Functions on Molecular Orbital Energies for Hydrocarbons. *Chem. Phys. Lett.* **1972**, *16*, 217–219. [CrossRef]
27. Hariharan, P.C.; Pople, J.A. The Influence of Polarization Functions on Molecular Orbital Hydrogenation Energies. *Theor. Chim. Acta.* **1973**, *28*, 213–222. [CrossRef]
28. Lee, C.; Yang, W.; Parr, R.G. Development of the Colle-Salvetti Correlation-Energy Formula into a Functional of the Electron Density. *Phys. Rev. B* **1988**, *37*, 785–789. [CrossRef]
29. Bondi, A. Van Der Waals Volumes and Radii. *J. Phys. Chem.* **1964**, *68*, 441–451. [CrossRef]
30. Yoshio, M.; Mukai, T.; Ohno, H.; Kato, T. One-Dimensional Ion Transport in Self-Organized Columnar Ionic Liquids. *J. Am. Chem. Soc.* **2004**, *126*, 994–995. [CrossRef]
31. The average number of molecules in a column stratum (μ) was estimated according to the following equation: $\mu = (N_A abh\rho)/M$, in which N_A is Avogadro's number, a and b is the lattice parameter (a = 42.1 Å and b = 38.4 Å), h is the thickness of the stratum (estimated to be ca. 3.7 Å, based on XRD analysis), ρ is the density (assumed to be 1 g cm^{-3}), and M is te molecular weight of RPNL 1·BSA.